Available online at www.sciencedirect.com
SCIENCE DIRECT®
Journal of Nuclear Materials 335 (2004) 48–58
journal of nuclear materials
www.elsevier.com/locate/jnucmat

Textural and microstructural developments during fabrication of Zr–2.5Nb pressure tubes

M. Kiran Kumar [a,*], C. Vanitha [a], I. Samajdar [a], G.K. Dey [b], R. Tewari [b], D. Srivastava [b], S. Banerjee [b]

[a] Department of Metallurgical Engineering and Material Science, IIT Bombay, Powai, Mumbai 400076, India
[b] Material Science Division, BARC, Trombay, Mumbai 400085, India

Received 9 March 2004; accepted 15 June 2004

Abstract

Zr–2.5wt%Nb pressure tubes, as used in the Indian pressurized heavy water reactors (PHWR), are fabricated through a combination of hot extrusion followed by two stages of cold pilgering and annealing. The present study makes an effort to systematically characterize the textural changes during the fabrication stages. The starting single-phase hcp martensitic structure was textured to start with and it also went through strong texture developments during hot extrusion. First and especially the second pilgering modified the texture. Such modifications were related to local discontinuity of the softer second phase, as an apparent continuity restricted lattice rotation in the primary hcp phase. Annealing caused discontinuity or spherodization of the bcc phase, but did not create recrystallization in the hcp matrix. The combination of two pilgering plus annealing operations, though the latter did not cause noticeable texture changes, however, reverted the final texture close to the parent hot-extruded texture.

1. Introduction

The fabrication of components with appropriate structure property has always been the real challenge to thermo-mechanical processing (TMP). A classical example is the selected component of the present study, the Zr–2.5wt%Nb pressure tube. This alloy is being increasingly used worldwide as pressure tube material for pressurized heavy water reactors of Candu design [1,2]. The Indian reactors are also now using the same material/component, albeit fabricated through a different sequence of TMP than the original Candu fabrication sequence [3,4]. Both fabrication routes are shown in Fig. 1 and earlier studies [3,4] had elaborated further on the modified TMP sequences of the Indian route, especially in terms of the overall microstructural developments.

The modifications in the TMP, as in Fig. 1, were expected to yield several advantages over conventional fabrication routes. Instead of an extrusion ratio of 11:1, as in the Candu TMP sequence, an 8:1 extrusion ratio was used. This required a two-stage pligering (or plug-rolling) with intermediate annealing steps (see Fig. 1). The sequence, though adequate for dimensional and overall microstructural developments, left several

* Corresponding author. Tel.: +91 22 25767621; fax: +91 22 25723480/25767621.
E-mail address: kaykay@met.iitb.ac.in (M. Kiran Kumar).

0022-3115/$ - see front matter © 2004 Elsevier B.V. All rights reserved.
doi:10.1016/j.jnucmat.2004.07.003

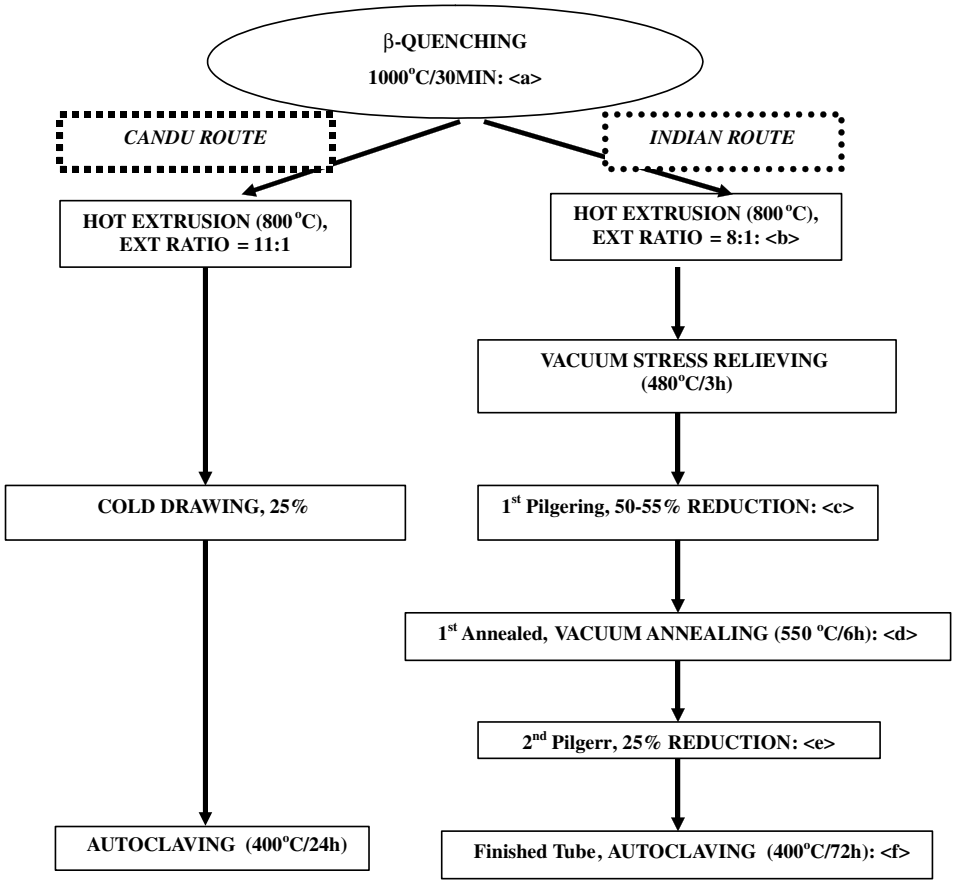

Fig. 1. Flow sheet for original Candu and the modified Indian TMP routes of Zr–2.5wt%Nb pressure tube fabrication. The following stages of the Indian route were studied: ⟨a⟩ β-quenched, ⟨b⟩ hot-extruded, ⟨c⟩ first pilger, ⟨d⟩ first annealed, ⟨e⟩ second pilger, ⟨f⟩ finished tube. The hot-extruded and the same material after vacuum stress relief are identical in terms of bulk texture and overall microstructure, the stress relief annealing was primarily to remove residual elastic stresses.

unanswered questions on the developments of bulk and microtexture. Texture strongly affects properties of the Zr based alloys, as used in the nuclear industry [1,2,5–16]. An optimized texture development is naturally one of the emphases in a TMP sequence. Texture developments have, however, one more important issue attached – it can be used to understand the mechanisms involved in the individual TMP stages as well [4]. Interestingly systematic studies, which are part of published literature, on the texture developments during the different TMP stages of fabrication of 2.5 Nb pressure tube do not exist. Usual understanding [4,15] was: the hot-extruded texture is carried through the cold deformation and annealing stages, final texture of the finished tube being equivalent to the parent hot-extruded texture. How far such understanding is quantitatively valid during individual TMP stages in the modified TMP sequence (see Fig. 1) for 2.5 Nb pressure tubes it is not really known. This is the basis for the present study.

2. Experimental methods

2.1. Material and processing

The detailed chemical composition of the Zr–2.5wt%Nb alloy is listed in Table 1, the pressure tube was fabricated through a sequence of TMP (see Fig. 1).

2.2. Characterization

The samples from different TMP stages, as marked in the caption of Fig. 1, were subjected to three different types of characterization – bulk texture measurements by X-ray diffraction (XRD), measurements of the XRD (2θ scans) peak broadening and microstructural/microtextural observations by transmission electron microscope (TEM). The first two observations were made in the mid-thickness sections of the extrusion planes, while TEM observations were carried out at

Table 1
Chemical composition of Zr–2.5%Nb alloy as used in the present study

Niobium (wt%)	Oxygen (ppm)	Iron (ppm)	Hydrogen (ppm)	Nitrogen (ppm)
2.51	1092	1250	<10	30

the mid-thickness of the long transverse (LT – containing extrusion and normal directions) planes.

For peak broadening a 2θ range of 10–100° scan, with Cu Kα radiation and a scan rate of 0.003° s^{-1} was used. A panalytical expert pro system with a fast detector was used in such scans and peak broadenings were estimated at full width (2θ angle) and half-maximum (FWHM) intensity. X-ray pole figures were measured on a Siemens D500 compatible goniometer. Orientation distribution functions (ODFs) were calculated by inversion of the four incomplete pole figures and using the standard series expansion [17]. The details of X-ray texture measurements are explained elsewhere [18]. The volume fractions of ideal texture/orientation components were estimated from discretized ODFs. TEM samples were prepared using standard electropolishing techniques [18], and the microtextural observations were made using TSL-ACT package in a Philips CM200 TEM.

3. Results

Samples were obtained from different stages of the Indian TMP sequence, as shown in Fig. 1. It is to be noted that the vacuum stress relieving, had no effects on the bulk texture and on the microstructure of the hot-extruded tube – the treatment being primarily used to relieve near surface residual stresses. The results on all other sequences are classified as the bulk observations, both peak broadening and bulk texture, and the microstructural observations, both microstructural and microtextural observations in TEM (except for the hot-extruded material, the 'fineness' of both the primary and the second phase restricted optical and SEM observations), and are presented accordingly.

3.1. Bulk observations

3.1.1. 2θ Scans

Fig. 2 shows the combined 2θ scans for the TMP stages. Such scans can provide a sense of gross textural changes, or changes in individual poles, and also changes in the respective peak broadening. The latter, taken with a parabolic fit at FWHM, can be treated as an index of relative hardening [19]. As shown in Fig. 2, considerable textural changes were observed during hot extrusion, while the integrity of the hot-extruded texture was qualitatively maintained during the subsequent TMP stages. This is, however, an incomplete and even inaccurate observation/statement, as shown in the subsequent bulk texture developments through X-ray ODFs.

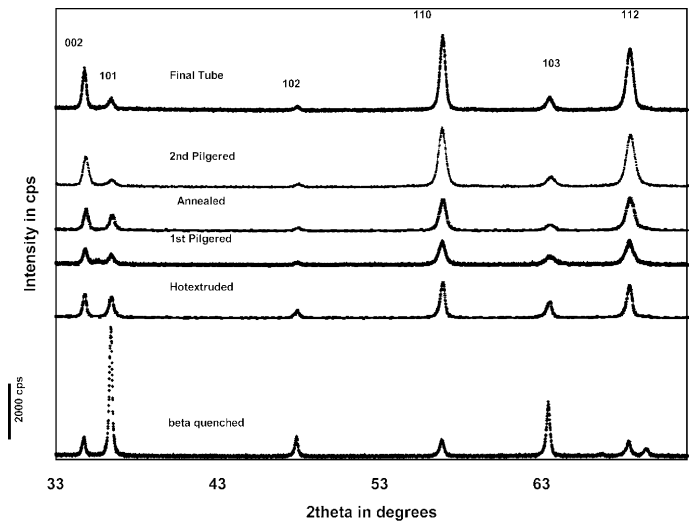

Fig. 2. 2θ XRD scans for samples from different TMP stages – stages as indicated in Fig. 1. (hkl) indices for the important α peaks are marked.

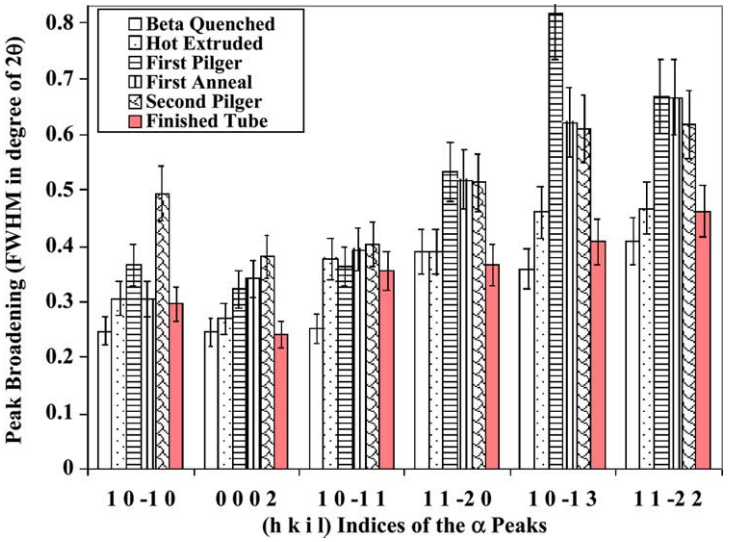

Fig. 3. Peak broadening (FWHM) data at different TMP stages for the marked α peaks in Fig. 2. An expected 10% error is marked by suitable error bars.

The peak broadening results are shown in Fig. 3. It is to be noted that the typical accuracy of such peak broadening estimates is considered to be about 10% of the estimated FWHM values – this probable 'inaccuracy' is marked on Fig. 3 with suitable error bars. The possible causes of this 'inaccuracy' are machine and software related and also related to the presence of the minority bcc β phase. The latter could not be indexed effectively, because of its very low volume fraction, in spite of the slow scan speed and the relatively efficient detector, and hence possible convolution of α and β peaks may arise in certain locations. In spite of the probable 'inaccuracy', one general trend is clear – pilgering broadened the peaks, or hardened the respective orientation components, while annealing had a softening effect. Deviations from this general trend fell well within the 10% inaccuracy.

3.1.2. Bulk texture

Fig. 4 shows the X-ray ODFs outlining the bulk texture developments during the different TMP stages. Fig. 5 extends the ODF observations through volume fraction developments of families of crystallographic planes. The estimated maximum ODF intensity, an index of 'texturing' [17], values are listed in Table 2. The observations on Figs. 4 and 5, and also of Table 2, can be summarized as:

- The β-quenched alloy has a non-random texture. Hot extrusion causes significant texture developments (Figs. 4 and 5) and also in 'texturing' (see Table 2). The hot-extruded texture can be roughly generalized as fiber-like texture with each fiber representing a family of orientations – specific crystallographic plane with all possible crystallographic directions on it.
- The subsequent TMP stages retain the semblance of the hot-extruded texture – though there were strong modifications in both texture and 'texturing' (Figs. 4 and 5 and Table 2). It is interesting to note, however, that the finished tube (after the second pilgering followed by autoclaving) had similar texture (including maximum ODF intensity) as that of the hot-extruded material.
- Other than the hot extrusion, first and the second pilgering cause the most significant textural changes (Figs. 4 and 5 and Table 2).

One of the important aspects of the bulk texture developments on properties is the relative concentration of the basal planes (or so-called basal texture) on the three planes – extrusion/rolling plane (RP) containing RD (rolling/extrusion direction) and TD (transverse direction), short transverse (ST) section containing ND (normal direction) and TD and the long transverse (LT) section containing RD and ND. Fig. 6 shows the volume fractions of basal fiber in all three cross-sections. For the hot-extruded alloy, the basal concentration is maximum at the rolling plane and least in LT/ST. The finished tube has a similar ratio, though there were changes in the intermediate TMP stages. This further confirms quantitatively that the parent hot-extruded texture is effectively reverted back in the finished tube, after two stages of pilgering and annealing.

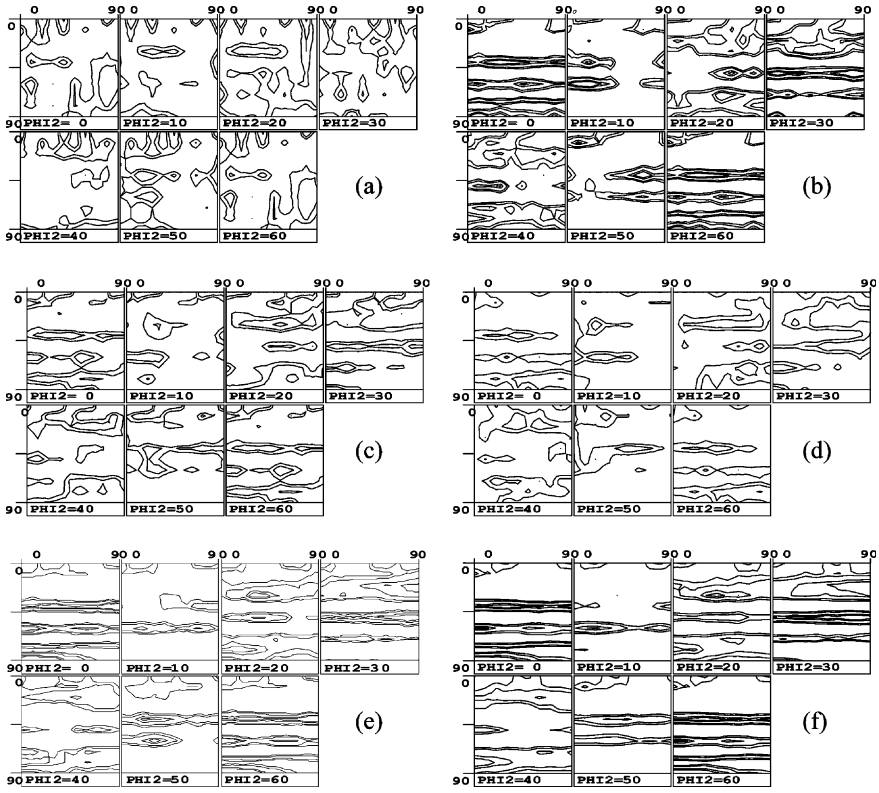

Fig. 4. ODFs representing the crystallographic texture of the hcp α phase at the different TMP stages, stages as marked in Fig. 1. Following contour levels (times random) are used for ODF plotting – 1.5, 2.5, 4.5, 5.5 and 8.7.

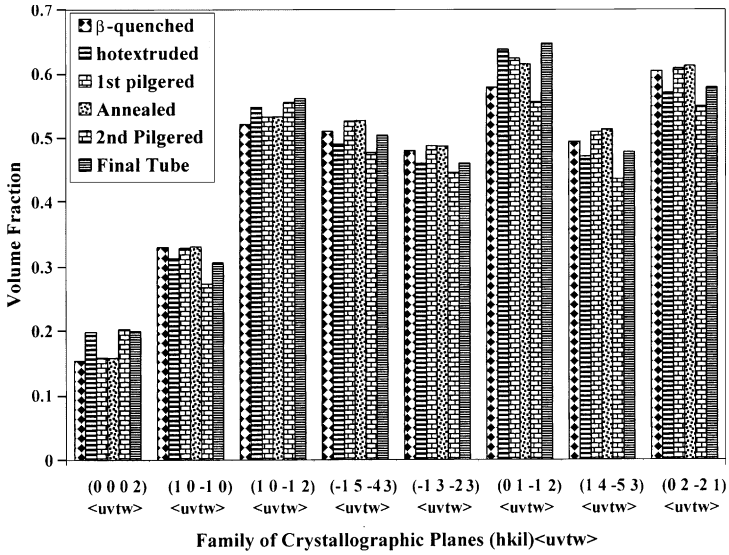

Fig. 5. Volume fractions of the idealized fibers (same crystallographic plane with all possible crystallographic directions in it), $(0002)\langle uvtw\rangle$, $(10\bar{1}0)\ \langle uvtw\rangle$, $(10\bar{1}2)\ \langle uvtw\rangle$, $(\bar{1}5\bar{4}3)\ \langle uvtw\rangle$, $(\bar{1}3\bar{2}3)\ \langle uvtw\rangle$, $(01\bar{1}2)\ \langle uvtw\rangle$, $(14\bar{5}3)\ \langle uvtw\rangle$ and $(02\bar{2}2)\ \langle uvtw\rangle$, at different TMP stages.

Table 2
Maximum X-ray ODF intensities at different TMP stages

Condition	Maximum ODF intensity
β-quenched	4.9
Hot-extruded	8.7
First pilgered	5.4
Annealed	4.7
Second pilgered	8.3
Final tube	8.2

3.2. Microstructural observations

Microstructural/microtextural observations were mostly obtained from LT plane (long transverse, though limited observations were made in other cross-sections as well). Following is a brief summary on the observations at the different processing stages. The β-quenched structure is discussed elsewhere [3].

3.2.1. Hot-extruded (⟨b⟩ as in Fig. 1)

Fig. 7 shows the stage ⟨b⟩ (as in Fig. 1) of the processing stage – hot-extruded material. Two types of hcp α grains were observed – relatively large single crystals/grains of α with 0.5–1 μm size along ND (often with high aspect ratio; aspect ratio of RD:ND typically range from 1:1 to 1:7 – an average of 1:3 was noted). Such α grains were often (but not always) surrounded by the bcc β phase. Relatively fine α grains, 0.1–0.2 μm in size, were observed with fine β dispersion in about 10–20% of the overall microstructure.

3.2.2. First pilgered (⟨c⟩ as in Fig. 1)

As in Fig. 8, the pilgering had a direct geometrical effect on the α grains – they were flattened/pancaked (average thickness varied between 0.2 and 0.5 μm). Shearing was quite apparent (pilgering has a complex tri-axial strain state) in several locations of the microstructure. Pilgering also highlighted the discontinuity in β and presence of deformed α without any visible β surrounding it. The microtexture developments in α grains did depend strongly on the presence/continuity of β. As shown in Fig. 8, in case of presence/continuity of the second phase, the α grain 'remained' single-crystalline and no new lattice curvature or high angle boundaries were observed. The so-called long range misorientation (LRM) [18] development was repetitive for such α. On the other hand, in case of noticeable absence or discontinuity in β (as shown in Fig. 8) the LRM development was cumulative and significant misorientation developments including high angle boundaries were observed in the deformed α. The TEM based microtexture measurements, as in Fig. 8, were aimed at bringing out the pattern of orientation changes and misorientation developments and should not be used as representative microtexture measurements to highlight stability of orientation(s). Statistically from TEM based microtexture this would be very difficult to index and was not attempted in the present study.

3.2.3. First pilgered plus vacuum annealed (⟨d⟩ in Fig. 1)

As in Fig. 9, the changes in microstructure were 'restricted', as the overall microstructure was not too different after annealing. The 'restricted' changes can be classified as 'limited' (in some locations) spherodization of β and recovery of α. The statement on recovery is made from the observations on the quality/sharpness of the Kikuchis – this improved noticeably after annealing. The average grain size (distance between high angle

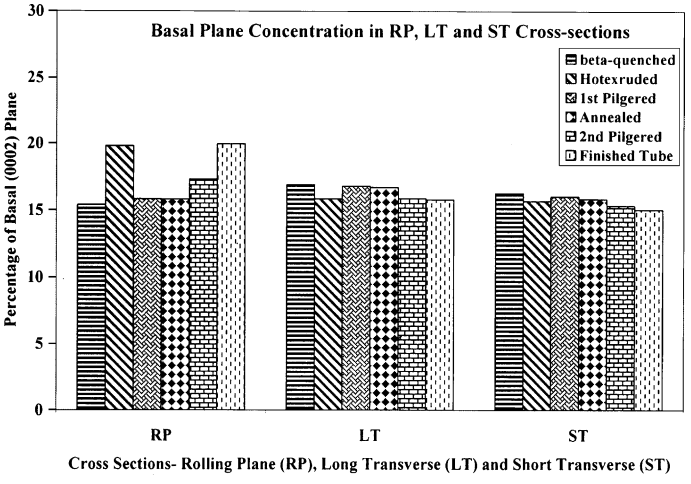

Fig. 6. Volume fraction (concentration) of basal plane, (0002) ⟨uvtw⟩, in all three cross-sections. rolling or extrusion plane (RP), long transverse (LT) and short transverse (ST) planes.

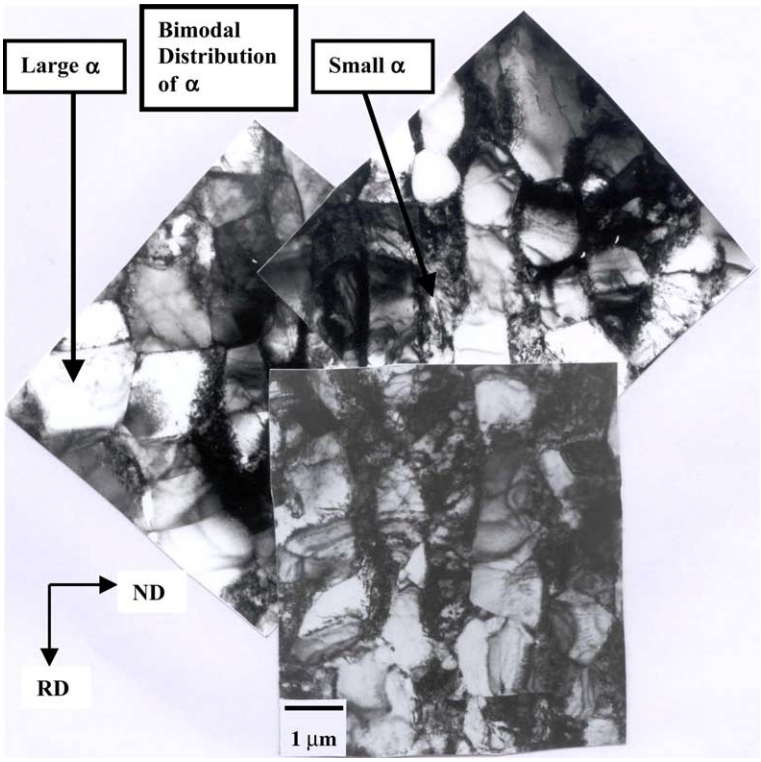

Fig. 7. Microstructure after hot extrusion. Bimodal grain size distribution of α is visible in the microstructure.

boundaries along ND), however, did not change significantly as compared to Fig. 8 (about 0.3 μm both before and after the annealing treatment), indicating the absence of significant recrystallization or grain growth at this stage.

3.2.4. Second pilgered (⟨e⟩ as in Fig. 1)

The second pilgering, with only 20–25% reduction in thickness, did bring out the β discontinuity more effectively (see Fig. 10). The thickness of α was not visibly affected (as compared to Fig. 9), explainable from the relatively minor reduction in thickness of 25%, as compared to 50–55% during first pilgering.

3.2.5. Finished tube (⟨f⟩ in Fig. 1)

Final autoclaving (see Fig. 11) did not modify the α size, again indicating the absence of recrystallization. However, the second phase was, often spherodized.

4. Discussion

As discussed earlier, the TMP sequence of the 2.5 Nb pressure tube was modified, in the so-called Indian route as given in Fig. 1. The processing stages in the modified sequence were, however, optimized based on the structural developments and their effects on the properties [3,4]. The present study provides an insight in the structural developments, in general, and textural/microtextural developments, in particular, during the individual processing stages:

- *Hot extrusion:* The β-quenching provided the starting single-phase martensitic structure [18], which was transformed during the hot extrusion with significant textural developments. The bimodal grain size distribution of the hot-extruded structure, as in Fig. 7, can be explained through β to α phase transformation. At the hot extrusion temperature, the β volume fraction is larger; so the large α plates are those which nucleated at early stages of hot extrusion. During cooling from the hot extrusion temperature, Zr-rich β transforms to α + Nb-rich β_{Nb}. These α plates would be small. This may explain the bimodal distribution of α. A similar example is often reported in steel [20] hot-rolled at temperatures where both austenite and ferrite are stable – the large ferrite grains evolve from deformation/recrystallization of ferrite, while the finer ferrite evolve from the austenite-to-ferrite transformation.
- *Pilgering:* The pilgering operations had a similar strain path and the strain was significantly lower in case of the second pilgering. Even then the textural modifications were equally strong for the second pligering, and at

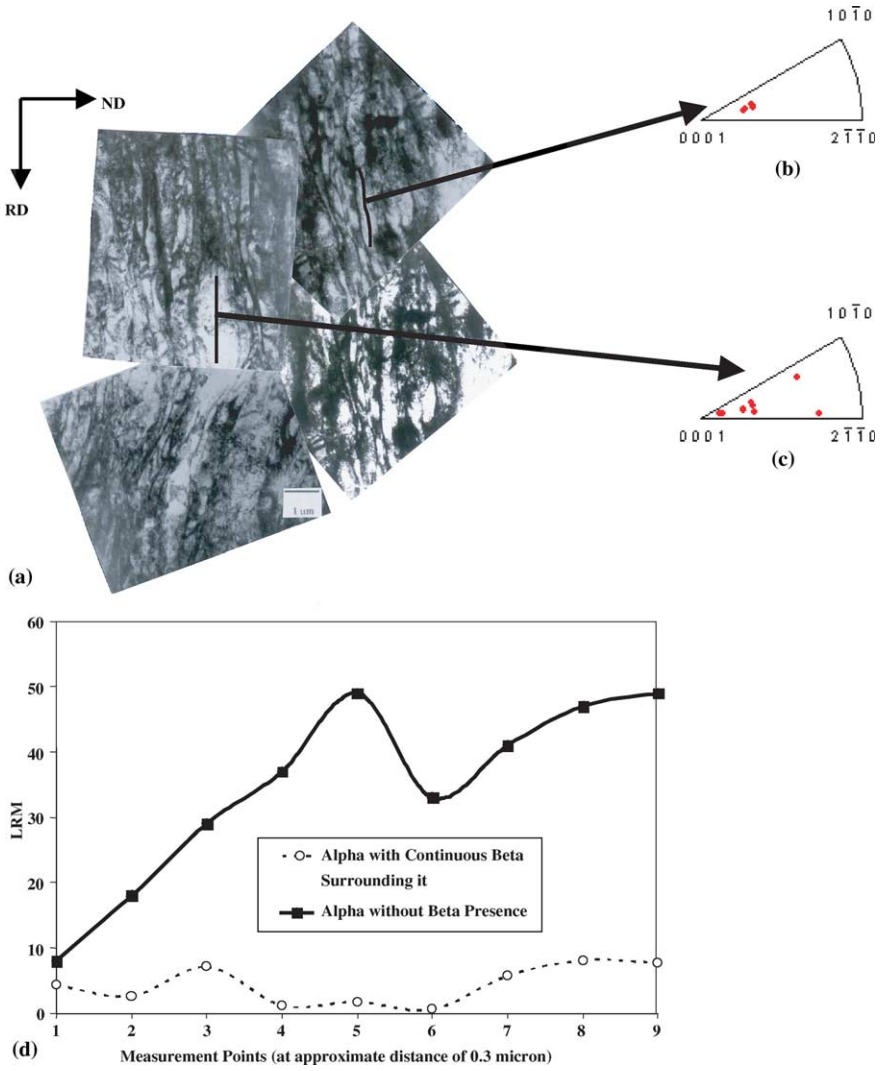

Fig. 8. (a) Microstructure after first pilgering. Local orientations were obtained along the lines marked in (a) and are shown as inverse pole figures respectively for regions (b) with and (c) without β continuity. LRM (long range misorientation [18], considered as the misorientation from origin) plots for (b) and (c) are shown in (d). It is to be noted that misorientation (among adjacent points) for (b) often exceeded 20°, while for (c) the average misorientation was 4° (and did not exceed 8°). These trends are representative.

times such modifications (as in the case of basal pole – Fig. 6) were opposite. If the deformation texture developments were governed by slip-twin activities alone, such changes cannot be explained. The only way to explain these, albeit qualitatively, is from the differences in the starting microstructure. Microtextural changes in both the pilgering stages were related to evolution of lattice rotations in regions with discontinuous presence of β (see Fig. 8). The apparent discontinuity being more in second pilgering was responsible for the strong texture developments during the same, though the strain was 'limited' as compared to the first pilgering. An extreme example of the β continuity in establishing the absence of textural developments is reported in a separate study [18] on Widmannstätten 2.5 Nb – where α plates had undergone no macroscopic strain, but only an in-plane rigid body rotation. Though macroscopic strain was present in the pilgered samples (see Fig. 8), but β continuity was clearly related to the absence of significant lattice rotations. In Widmannstätten 2.5 Nb with β continuity and no macroscopic strain [18], an absence of qualitative or quantitative texture development was observed. However, for the present material, sluggish (sluggish as compared to single-phase [18]) texture modifications were noted. The only way to explain this is to consider that the second phase acted more like strain

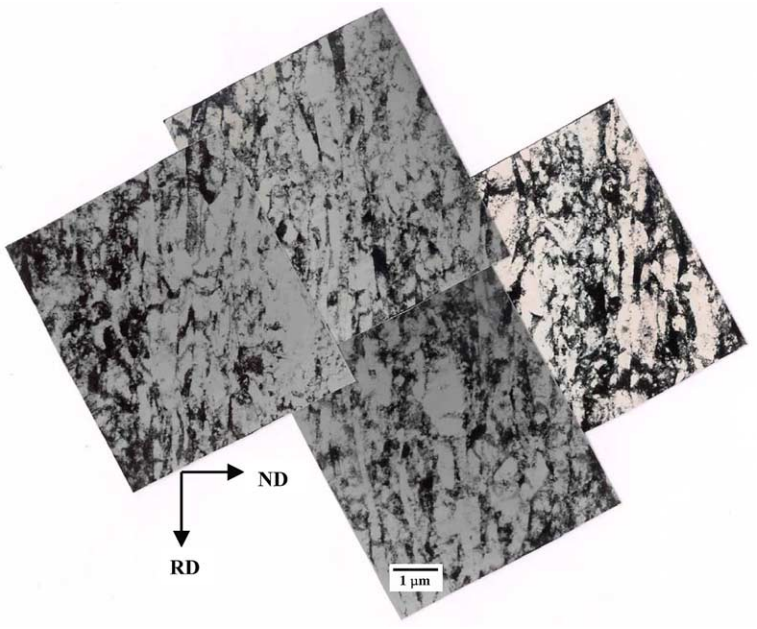

Fig. 9. Microstructure after first annealing indicating spherodization of β. The thickness of the α, however, did not change noticeably – indicating the absence of noticeable recrystallization.

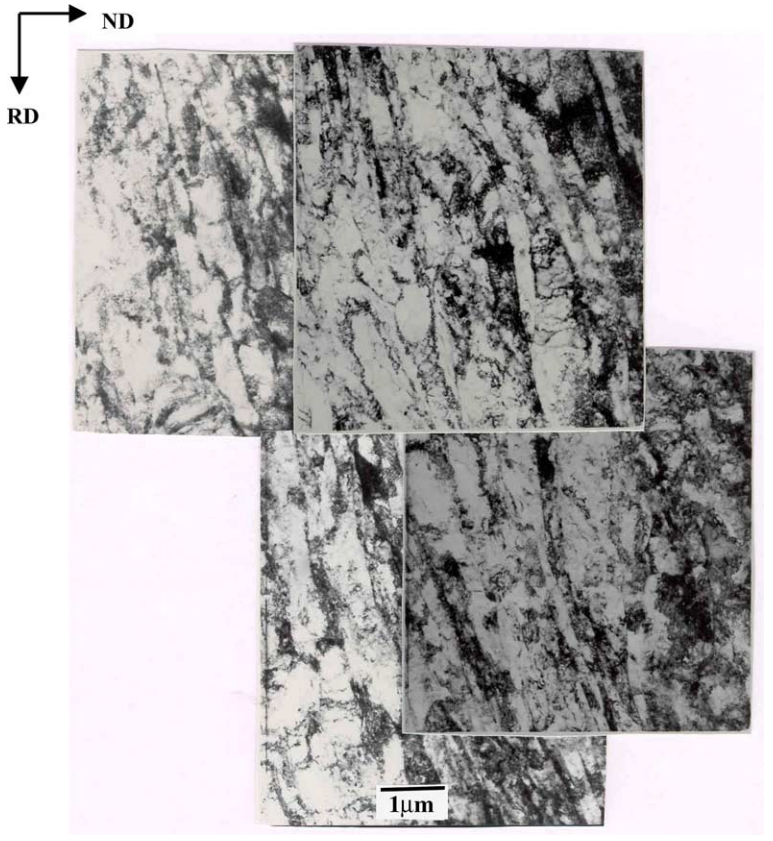

Fig. 10. Regions of β discontinuity were more apparent after the second pilgering. However, the change in grain (α) size was, not too evident, the strain being limited to 25% reduction in thickness.

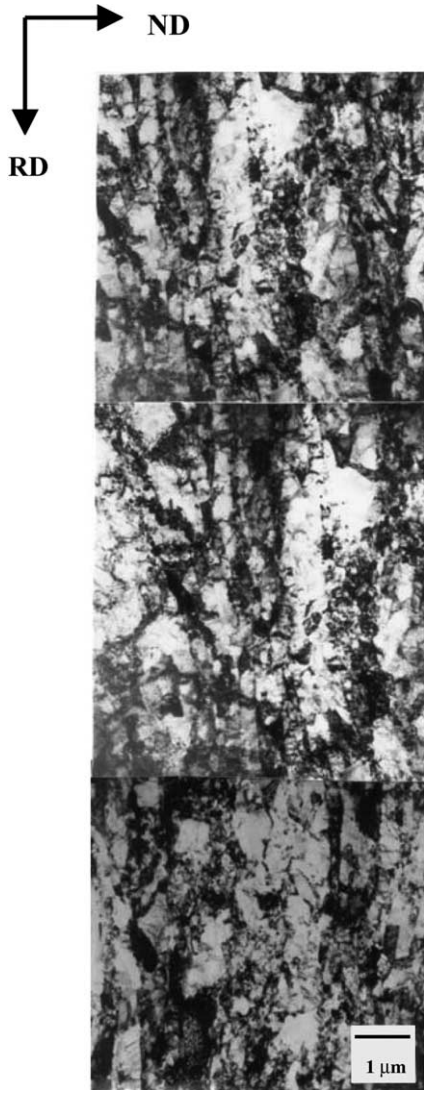

Fig. 11. Microstructure of the finished tube. No significant changes in grain (α) size (and no noticeable recrystallization or grain growth), but spherodization of β were evident.

localizations, where the majority of deformation/dislocation activities were restricted, leaving the adjacent hcp matrix free from significant lattice rotations and texture developments.

- *Annealing*: Both annealing treatments resulted in reduced dislocation densities, as indicated by reduced peak broadening and the microstructural evidence, including clarity/presence of Kikuchi patterns. The lack of changes in α grain size and also in bulk texture developments during both the annealing steps, however, clearly establish the absence of any significant recrystallization. The average grain size of the α phase (along ND) was about 0.3 μm, both before and after the first annealing treatment. That means no noticeable recrystallization even in the heavily deformed tubes. This was due to pinning (Zener pinning) by the second phase β. Continuous dynamic recrystallization is a possibility during hot extrusion, but not in the latter fabrication stages. Continuous recrystallization during static annealing and/or deformation (or extended recovery), though common in single-phase zirconium based alloys, were not observed in the present two-phase system. The suppression of new cell walls or sub-boundaries in the 0.2–0.3 μm range of the α grains (and with β continuity) and sub-grain formation in case of β discontinuity were observed. The latter was dominant during annealing, as annealing did bring a relatively larger extent of β discontinuity through spherodization of the second phase. Spherodization after the first annealing (see Fig. 9) was responsible for more α–α interactions leading to strong textural changes during the second pilgering with only 25% reduction.

In summary, texture of the hot-extruded material could be 'brought back' by a combination of two-stage pilgering and annealing. The crucial factor for significant textural developments during both the pilgering was the discontinuity in the second phase β. The absence of recrystallization during annealing is related to the relative absence of high-angle boundaries created during respective pilgering and also from pinning by the second phase.

5. Summary

- Significant development in crystallographic texture was obtained through hot extrusion. Subsequent two-stage pilgering plus annealing process 'brought back' the hot-extruded texture, though there were changes during individual pilgering stages.
- The hot-extruded microstructure had a bimodal size distribution for hcp α grains – the possible source of fine α grains being β-to-α transformation.
- The effectiveness of pilgering on texture/microtexture development did depend on the relative presence/continuity of the second phase β. In case of β continuity, the lattice rotations were restricted limiting the misorientation developments (and also developments in bulk texture) of the α grains. Relatively more β discontinuity during the second pilgering explains a strong texture development with only 25% reduction in thickness (as compared to 50–55% in the first pilgering).
- Other than relative spherodization of β, annealing did not bring any noticeable recrystallization, hence no significant changes in texture and α grain size were observed. Relative softening during annealing, as evident from reduced X-ray peak broadening, was mainly through recovery.

Acknowledgments

The authors would like to acknowledge BRNS (Board of Research in Nuclear Sciences) for financial support and NFC (Nuclear Fuel Complex) for supplying the material. DST (Department of Science and Technology) is acknowledged for the TEM based local orientation measurement set-up and SAIF (Sophisticated Analytical Instrumentation Facility), IIT Bombay, for the support in TEM studies.

References

[1] C.O. Smith, Nuclear Reactor Materials, Addision-Wesley, 1967, p. 130.
[2] G. Maussner, E. Ortlieb, H.G. Weidinger, Materials for Nuclear Reactor Core Applications, BNES, London, 1987, p. 49.
[3] D. Srivastava, G.K. Dey, S. Banerjee, Bhabha Atomic Research Centre, Bombay Technical Report, BARC/1992/I/011, 1992.
[4] D. Srivastava, G.K. Dey, S. Banerjee, Metall. Mater. Trans. 26A (1995) 2707.
[5] F. Prat, M. Grange, J. Besson, E. Andrieu, Metall. Mater. Trans. 29A (1998) 1643.
[6] J.B. Bai, N. Ji, D. Gilbon, J.L. Lebrun, Scr. Metall. Mater. 26 (1992) 369.
[7] D.H. Lee, S.I. Kwun, Scr. Metall. Mater. 31 (1994) 1475.
[8] S.K. Hwang, H.S. Ryoo, J.W. Morris Jr., Metall. Trans. 22A (1991) 2247.
[9] R.A. Holt, J. Nucl. Mater. 82 (1979) 419.
[10] E.F. Ibrahim, R.A. Holt, J. Nucl. Mater. 91 (1980) 311.
[11] R.A. Holt, E.F. Ibrahim, Acta Met. 27 (1979) 1319.
[12] B.A. Cheadle, C.E. Ells, W. Evans, J. Nucl. Mater. 23 (1967) 199.
[13] E.F. Ibrahim, J. Nucl. Mater. 118 (1983) 260.
[14] V. Perovic, G.C. Weatherly, C.J. Simpson, Acta Met. 31 (1983) 1381.
[15] A. Salinas Rodriguez, J.J. Jonas, Metall. Trans. 23A (1992) 271.
[16] K. Linga Murty, R. Jallepalli, S.T. Mahmood, Nucl. Eng. Des. 148 (1994) 1.
[17] J. Bunge, Texture Analysis in Materials Science, Butterworths, London, 1982.
[18] M. Kiran Kumar, I. Samajdar, N. Venkatramani, G.K. Dey, R. Tewari, D. Srivastava, S. Banerjee, Acta Met. Mater. 51 (2003) 625.
[19] B.D. Cullity, Elements of X-Ray Diffraction, 2nd Ed., Addison-Wesley, 1978, p. 460.
[20] S. Cicalè, I. Samajdar, B. Verlinden, G. Abbruzzese, P. Van Houtte, ISIJ Int. 42 (2002) 770.